Essential elements for nuclear binding

Bing-Nan Lu,[1] Ning Li,[1] Serdar Elhatisari,[2,3] Dean Lee,[1] Evgeny Epelbaum,[4] and Ulf-G. Meißner[2,5,6]

[1]*Facility for Rare Isotope Beams and Department of Physics and Astronomy, Michigan State University, MI 48824, USA*
[2]*Helmholtz-Institut für Strahlen- und Kernphysik and Bethe Center for Theoretical Physics, Universität Bonn, D-53115 Bonn, Germany*
[3]*Department of Engineering, Karamanoglu Mehmetbey University, Karaman 70100, Turkey*
[4]*Ruhr University Bochum, Faculty of Physics and Astronomy, Institute for Theoretical Physics II, D-44870 Bochum, Germany*
[5]*Institute for Advanced Simulation, Institut für Kernphysik, and Jülich Center for Hadron Physics, Forschungszentrum Jülich, D-52425 Jülich, Germany*
[6]*Tbilisi State University, 0186 Tbilisi, Georgia*

How does nuclear binding emerge from first principles? Our current best understanding of nuclear forces is based on a systematic low-energy expansion called chiral effective field theory. However, recent *ab initio* calculations of nuclear structure have found that not all chiral effective field theory interactions give accurate predictions with increasing nuclear density. In this letter we address the reason for this problem and the first steps toward a solution. Using nuclear lattice simulations, we deduce the minimal nuclear interaction that can reproduce the ground state properties of light nuclei, medium-mass nuclei, and neutron matter simultaneously with no more than a few percent error in the energies and charge radii. We find that only four parameters are needed. The first two determine the strength and range of the two-nucleon forces. The third controls the strength of the three-nucleon contact interaction. While these three parameters are already part of the standard chiral effective field theory program, the fourth and last parameter is a new feature that controls the strength of the local part of the nuclear interactions. By the term local we mean an interaction that is velocity independent. With these four parameters one can accurately describe neutron matter up to saturation density and the ground state properties of nuclei up to calcium. We discuss the impact of these findings for future *ab initio* calculations using chiral effective field theory and the resurgence of Wigner's approximate SU(4) symmetry in nuclear binding.

A first principles approach to nuclear forces is provided by chiral effective field theory (χEFT), where interactions are arranged as a low-energy expansion in powers of momentum and pion mass. The nucleon-nucleon (NN) and three-nucleon (3N) interactions are determined by fitting to experimental data on NN scattering and 3N observables [1–6]. See Refs. [7–9] for review articles. χEFT has been combined with state-of-the-art computational algorithms and powerful supercomputers to produce a wealth of new predictions and insights into nuclear structure and reactions. While many calculations establish the reliability of χEFT in light nuclei [10–14], some problems have been found for the binding energies and charge radii of medium mass nuclei [13, 15–17].

The core issue is that χEFT many-body calculations do not yet give reliable and accurate predictions at higher nuclear densities. If one reaches high enough orders in the χEFT expansion, then the problems are expected to be resolved. Many-nucleon forces start contributing at higher orders and can tame the problems appearing at higher nuclear densities. However, the number and complexity of these many-nucleon interactions are enormous, and a systematic treatment of such effects is not yet practical. It can also not be excluded that these complications can be avoided by a clever rearrangement of the power counting, see e.g. [18, 19].

One pragmatic approach is to further constrain the nuclear force using nuclear structure data from medium mass nuclei or the saturation properties of nuclear matter [20–23]. This approach has been applied successfully in several recent calculations [24–27]. A rather different line of investigation has looked at the microscopic origins of the problem. In Ref. [28] numerical evidence is shown that nuclear matter sits near a quantum phase transition between a Bose gas of alpha particles and nuclear liquid. It is argued that local SU(4)-invariant forces play an increasingly important role at higher nuclear densities, and this could explain why some χEFT many-body calculations are successful while others are not. The term local refers to velocity-independent interactions, and the SU(4) is Wigner's approximate symmetry of the nuclear interactions where nucleons can be regarding as four components of an SU(4) multiplet [29].

The lightest system where local SU(4)-invariant forces play an important role is in the scattering between two alpha particles. The importance of local SU(4)-invariant interactions at higher densities can be explained in terms of coherent enhancement. SU(4)-invariant interactions are enhanced because spin-dependent forces tend to cancel when summing over closed shells and isospin-dependent forces tend to cancel in symmetric nuclear matter. Local interactions are enhanced because each nucleon can interact with its surrounding nucleons without disturbing its local quantum environment. The special role of local forces has been studied in some depth by looking at the effective interactions between two bound dimers in a one-dimensional model [30].

The idea of SU(4) universality at large S-wave scattering length has a rich history in nuclear physics. It is well known that the Tjon line relating ^{3}H and ^{4}He binding energies is a manifestation of universality in nuclear systems [31, 32]. It has also been shown that ^{3}H and ^{4}He are characterized by universal physics associated with the Efimov effect [33, 34]. The importance of SU(4)-invariant forces at higher densities suggests a possible resurgence of SU(4) invariance for short-range nuclear forces in the many-body environment. This idea

inspired the exploratory work in Ref. [35] on the structure of nuclei up through oxygen using an SU(4)-invariant interaction.

In this work we attempt to tie all of the loose threads together. We take a constructive reductionist approach and deduce the minimal nuclear interaction that can reproduce the ground state properties of light nuclei, medium-mass nuclei, and neutron matter simultaneously with no more than a few percent error in the energies and charge radii. We then discuss the impact on *ab initio* calculations using chiral effective field theory and the importance of Wigner's approximate SU(4) symmetry.

We start with a simple SU(4)-invariant leading order effective field theory without explicit pions (pion-less EFT) on a periodic L^3 cube with lattice coordinates $\boldsymbol{n} = (n_x, n_y, n_z)$. The Hamiltonian is

$$H_{\mathrm{SU(4)}} = H_{\mathrm{free}} + \frac{1}{2!}C_2 \sum_{\boldsymbol{n}} \tilde{\rho}(\boldsymbol{n})^2 + \frac{1}{3!}C_3 \sum_{\boldsymbol{n}} \tilde{\rho}(\boldsymbol{n})^3, \quad (1)$$

where H_{free} is the free nucleon Hamiltonian with nucleon mass $m = 938.9$ MeV. The density operator $\tilde{\rho}(\boldsymbol{n})$ is defined in the same manner as in Ref. [35],

$$\tilde{\rho}(\boldsymbol{n}) = \sum_i \tilde{a}_i^\dagger(\boldsymbol{n})\tilde{a}_i(\boldsymbol{n}) + s_L \sum_{|\boldsymbol{n}'-\boldsymbol{n}|=1} \sum_i \tilde{a}_i^\dagger(\boldsymbol{n}')\tilde{a}_i(\boldsymbol{n}'), \quad (2)$$

where i is the joint spin-isospin index and the smeared annihilation and creation operators are defined as

$$\tilde{a}_i(\boldsymbol{n}) = a_i(\boldsymbol{n}) + s_{NL} \sum_{|\boldsymbol{n}'-\boldsymbol{n}|=1} a_i(\boldsymbol{n}'). \quad (3)$$

The summation over the spin and isospin implies that interaction is SU(4) invariant. The parameter s_L controls the strength of the local part of the interaction, while s_{NL} controls the strength of the nonlocal part of the interaction. Here we include both kinds of smearing. Both s_L and s_{NL} have an impact on the range of the interactions. The parameters C_2 and C_3 give the strength of the two-body and three-body interactions, respectively.

In this letter we use a lattice spacing $a = 1.33$ fm, which corresponds to a momentum cutoff $\Lambda = \pi/a \approx 465$ MeV. The dynamics with momentum Q much smaller than Λ can be well described and residual lattice artifacts are suppressed by powers of Q/Λ [36, 37]. In Ref. [38] we showed that the NN scattering phase shift can be precisely extracted on the lattice using the spherical wall method. In this work we fix the two-body interaction by fitting the scattering length a_0 and effective range r_0. In each instance we calculate the NN S-wave phase shifts below relative momentum $P_{\mathrm{rel}} \leq 50$ MeV using the spherical wall method and calculate fit errors by comparing results with the effective range expansion given by the targeted (a_0, r_0) values and update parameters correspondingly using the Levenberg-Marquardt algorithm. This process is repeated until full convergence is achieved.

For $A \geq 3$ the ground state of the lattice Hamiltonian Eq. (1) can be determined non-perturbatively using the framework of lattice effective field theory [39–42]. Here we briefly give parameters used in this work. We impose cubic periodic boundaries with length L. For nuclei with $A < 30$ we take $L \geq 8$, with larger values of L for cases where more accuracy is desired. For nuclei with $A \geq 30$ we take $L = 9$. The temporal lattice spacing is 0.001 MeV^{-1} and projection time is set to 0.3 MeV^{-1}. We found that these settings give reliable results for the ground states with $A \leq 48$. Recently we also developed a pinhole algorithm which enables us to calculate the density profiles and charge radii on the lattice with high precision [35]. These algorithms together provide a powerful tool box for analyzing nuclear systems from NN scattering to nuclear structures.

First we fix the parameters C_2, C_3, s_L using few-body data. As the two parameters s_L and s_{NL} are interchangeable in the few-body sector [28], we can simply set $s_{NL} = 0.5$ in this section. The remaining local smearing constant s_L and two-body interaction strength C_2 can be unambiguously determined by fitting to the S-wave scattering length a_0 and effective range r_0. As these constants have different values in $^1S_0$ and $^3S_1$ channels, we have to determine what are the proper averages to use for our SU(4) interactions. As $r_0(^1S_0) = 2.77$ fm and $r_0(^3S_1) = 1.75$ fm are not too far from each other, we simply set $r_0 = (r_0(^1S_0) + r_0(^3S_1))/2 \approx 2.2$ fm.

In order to tune the SU(4)-averaged scattering length a_0, we consider corrections that arise from inclusion of SU(4)-breaking $^1S_0$ and $^3S_1$ contact interactions and adjust a_0 to minimize the size of these corrections to the ^{3}H and ^{4}He binding energies. This process gives an optimal value of $a_0 = 9.1$ fm, and we use this value of a_0 in what follows. We note that our deuteron is degenerate with a di-neutron state and the binding energy is an SU(4) average of the $^1S_0$ and $^3S_1$ sectors, and thus has less than half of the physical deuteron binding energy. However this issue is quite easily fixed when SU(4)-breaking interactions are introduced.

With C_2 and s_L fixed by a_0 and r_0, the three-body force strength C_3 can be determined in the usual manner by fitting to the ^{3}H binding energy. At the physical point where we get the physical value $B(^3\mathrm{H}) = 8.48$ MeV, the ^{4}He binding energy with the Coulomb interaction included is 28.9 MeV. This is close to the experimental value $B(^4\mathrm{He}) = 28.3$ MeV, and the remaining discrepancy is consistent with the expected size of higher order contributions and SU(4)-breaking effects.

The remaining parameter not fixed by the few-body data is s_{NL}. For different values of s_{NL} we repeated the above procedures to generate a group of interactions with different strengths for the local part of the interaction. We obtained five such interactions with s_{NL} =0.40, 0.45, 0.50, 0.55 and 0.60 and denote them as NL40, NL45, NL50, NL55, and NL60, respectively. We note that since the effective range is kept constant, decreasing s_{NL} corresponds to increasing s_L and thus the strength of the local part of the interaction. While we used alpha-alpha scattering to fix the local part of the interaction in Ref. [28], we are aware that such scattering calculations are difficult for other *ab initio* methods to reproduce. Therefore we adopt a different approach that looks at the ground state energies of medium mass nuclei.

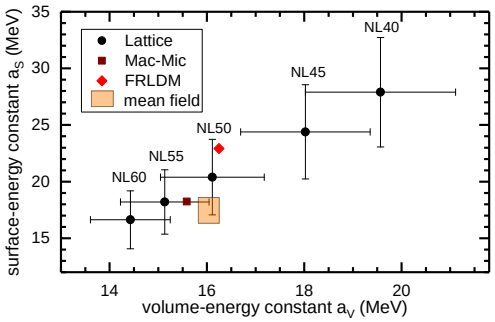

Figure 1. The correlation plot for the calculated volume-energy constant a_V and surface-energy constant a_S. The square, diamond and square region denote the results fitted with Macroscopic-Microscopic model [44], Finite Range Liquid Drop Model [43], Mean Field Models [45], respectively.

For medium mass nuclei with $A \geq 16$, the binding energies can be well parameterized with the Bethe-Weizsäcker mass formula,

$$B(A) = a_V A - a_S A^{\frac{2}{3}} + E_{\rm Coulomb} + \cdots , \qquad (4)$$

where a_V and a_S are volume-energy and surface-energy constants, respectively, $E_{\rm Coulomb}$ is the Coulomb energy, and the ellipsis represents the symmetry energy, pairing energy, shell correction energy, etc. To avoid fitting complexities not accurately captured in our minimal nuclear interaction, we fit only $N = Z$ even-even nuclei, for which the symmetry energy vanishes and the pairing energy varies smoothly. The shell correction energy is known to be much smaller than the macroscopic contribution in this mass region [43] and thus the first three terms appearing in Eq. (4) dominate.

For each interaction we use the calculated binding energies with $16 \leq A \leq 40$ to extract the liquid drop constants a_V and a_S. We observe prominent shell effects for these nuclei, and the binding energy per nucleon fluctuates around the liquid drop values with maxima at the magic numbers. In the fitting procedure the shell effects across a whole shell are averaged out, thus decreasing uncertainties for the liquid drop constants. The a_S-a_V plot is shown in Fig. 1. We can see a linear correlation between these constants. The values of a_S and a_V both increase as the strength of the local part of the interaction increases. For comparison, we also show other values of these constants in the literature, in which the masses throughout the whole nuclide chart are used in the fits. We found that the interaction NL50 gives a value of a_V closest to other estimations. This value of a_V still gives an estimate of the energy per nucleon at saturation. The uncertainty in a_S is large but still matches the empirical values.

In Table I we show the binding energies and charge radii for selected nuclei. For comparison we also list the experimental values and the calculated Coulomb energy. While the ^{3}H energy is exact due to the fitting procedure, all the other values are predictions. The largest relative error in binding energy 4.5% occurs for ^{16}O. While most of the charge radii are overestimated, the largest relative error is only 8.0% and occurs for ^{3}H. For the lattice calculations of the nuclear charge radii, we have taken into account the charge radius of the proton.

Table I. The calculated binding energies and charge radii of ^{3}H, ^{3}He and selected alpha-like nuclei compared with experimental values. The Coulomb interaction is taken into account perturbatively. All energies are in MeV and radii in fm. Experimental binding energies are taken from Ref. [47] and radii from Ref. [48].

	B	Exp.	$R_{\rm ch}$	Exp.	Cou.
^{3}H	8.48(2)	8.48	1.90(1)	1.76	0.0
^{3}He	7.75(2)	7.72	1.99(1)	1.97	0.73(1)
^{4}He	28.89(1)	28.3	1.72(1)	1.68	0.80(1)
^{16}O	121.9(1)	127.6	2.74(1)	2.70	13.9(1)
^{20}Ne	161.6(1)	160.6	2.95(1)	3.01	20.2(1)
^{24}Mg	193.5(2)	198.3	3.13(1)	3.06	28.0(1)
^{28}Si	235.8(4)	236.5	3.26(1)	3.12	37.1(2)
^{40}Ca	346.8(6)	342.1	3.42(1)	3.48	71.7(4)

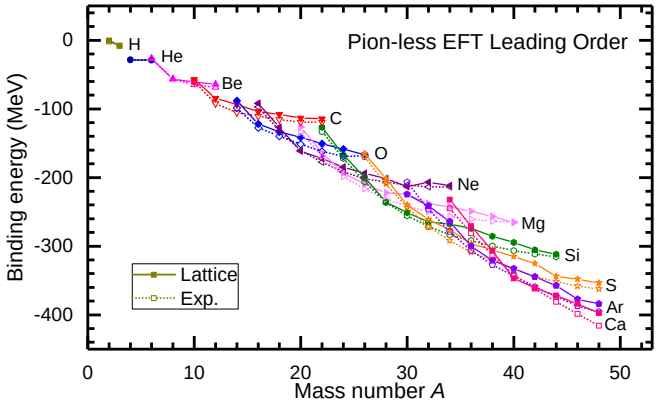

Figure 2. The calculated binding energies from ^{3}H to ^{48}Ca. The solid symbols denote the lattice results and the open symbols denote the experimental values. Different symbols and colors denote different element. The Coulomb interaction is taken into account perturbatively. The experimental values are taken from Ref. [47].

In order to examine the global behavior, here we calculate the binding energies for totally 86 even-even nuclei up to A=48. For each isotope chain we only consider the nuclides known to be bound in experiments. The results are shown and compared with the data in Fig. 2. Because the interaction has an exact SU(4) symmetry, we are free of the sign problem and can calculate the binding energies with high precision. In Fig. 2 all of the Monte Carlo error bars are smaller than the size of the symbols. The remaining errors due to imaginary time and volume extrapolations are also small but not explicitly shown in the plot. In Fig. 2 we see that the gross feature of the binding energies along each isotopic chain are well reproduced. In particular, the slopes of each isotopic curve on the proton-rich side are close to experimental value. However, since we are using a simple central force without any spin or isospin dependence, the discrepancy is somewhat larger on the neutron-rich side.

The charge density profile is another important physical

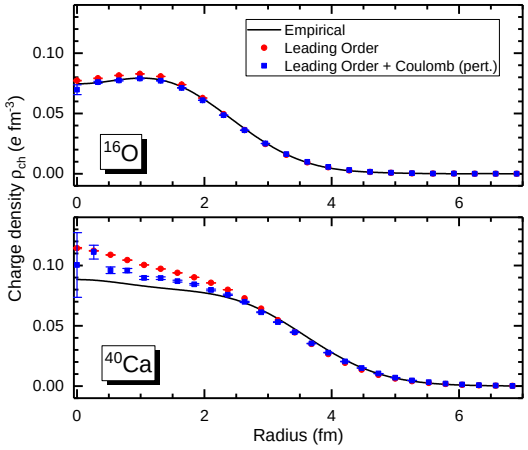

Figure 3. The calculated ^{16}O and ^{40}Ca charge densities compared with the empirical results. The circles denote the results without Coulomb interaction. The squares denote the results with the Coulomb interaction included perturbatively. Empirical values are taken from Ref. [49].

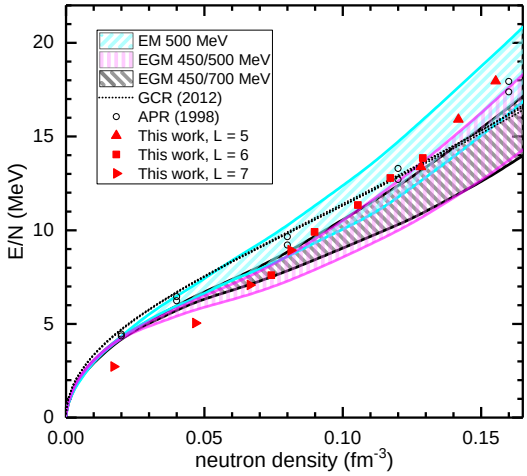

Figure 4. The pure neutron matter (NM) energy as a function of neutron density calculated using the NL50 interaction with box size L=5 (up triangles), L=6 (squares), L=7 (right triangles), respectively. For comparison we also show results calculated with full N^{3}LO chiral interactions (EM 500 MeV, EGM 450/500 MeV and EGM 450/700 MeV) [50], the results from variational (APR) [51] and Auxiliary Field Diffusion MC calculations (GCR) [52].

quantity sensitive to the nuclear interaction. In Fig. 3 we show the charge densities of ^{16}O and ^{40}Ca calculated with the pinhole algorithm. We have again taken into account the charge distribution of the proton. To compare with data from the electron scattering experiments we also show the results with the Coulomb interaction included with first order perturbation theory. For both nuclei, the charge densities without Coulomb interaction show clear Gaussian shapes. The center densities of ^{16}O and ^{40}Ca are approximately 0.08 e·fm^{-3} and 0.11 e·fm^{-3}, respectively. The Coulomb force suppresses the center densities and expands the nuclei, drawing the results closer to the empirical data. Our results are surprisingly good for such as a simple nuclear interaction.

Finally we examine the predictions for pure neutron matter (NM). In Fig. 4 we show the calculated NM energy as a function of the neutron density compared with other calculations. Here we use three different box size $L = 5, 6, 7$ with neutron numbers varying from 14 to 66. We compare our results with other calculations with full N^{3}LO chiral interactions. We see that our results are in line with the other calculations at densities above 0.05 fm^{-3}. At lower densities the discrepancy is larger because our SU(4)-invariant interaction is not tuned to the physical neutron-neutron scattering length, but this is simply fixed by including SU(4)-breaking interactions. Overall, our results are quite good in view of the simplicity of the interaction.

In this letter we have shown that the ground state properties of light nuclei, medium-mass nuclei, and neutron matter can be described using a minimal nuclear interaction with only four interaction parameters. While the first three parameters are already standard in χEFT, the fourth and last parameter is a new feature that controls the strength of the local part of the nuclear interactions. We expect that these new insights might help design new χEFT calculations with better convergence at higher densities. While in this analysis we are controlling the strength of the local part of the interactions primarily through the NN interaction, we suspect that one could also control the local part of the interactions at the 3N level only. This may explain the large differences seen in recent *ab initio* calculations using different 3N forces.

Aside from the Coulomb interaction, all of the other interactions in this minimal model obey Wigner's SU(4) symmetry. This seems to be an example of emergent universality. The SU(4) interaction resurges at higher densities not because the underlying fundamental interaction is invariant, but because the SU(4) interaction is coherently enhanced in the many-body environment. This is not to minimize the important role of spin-dependent effects such as spin-orbit couplings and tensor forces. However, it does seem to suggest that SU(4) invariance plays a key role in the bulk properties of nuclear matter.

Acknowledgements We thank A. Schwenk for providing the neutron matter results for comparison. We acknowledge partial financial support from the Deutsche Forschungsgemeinschaft (SFB/TRR 110, "Symmetries and the Emergence of Structure in QCD"), the BMBF (Grant No. 05P15PCFN1), the U.S. Department of Energy (DE-SC0018638 and DE-AC52-06NA25396), and the Scientific and Technological Research Council of Turkey (TUBITAK project no. 116F400). Further support was provided by the Chinese Academy of Sciences (CAS) President's International Fellowship Initiative (PIFI) (grant no. 2018DM0034) and by VolkswagenStiftung (grant no. 93562). The computational resources were provided by the Julich Supercomputing Centre at Forschungszentrum Jülich, Oak Ridge Leadership Computing Facility, RWTH Aachen, and Michigan State University.

[1] D. R. Entem and R. Machleidt, Phys. Rev. C 68, (2003).
[2] E. Epelbaum, W. Glöckle, and U.-G. Meißner, Nucl. Phys. A 747, 362 (2005).
[3] E. Epelbaum, A. Nogga, W. Glöckle, H. Kamada, U.-G. Meißner, and H. Witała, Phys. Rev. C 66, 064001 (2002).
[4] E. Epelbaum, H. Krebs and U.-G. Meißner, Phys. Rev. Lett. **115**, no. 12, 122301 (2015).
[5] P. Reinert, H. Krebs and E. Epelbaum, Eur. Phys. J. A **54**, no. 5, 86 (2018).
[6] D. R. Entem, R. Machleidt and Y. Nosyk, Phys. Rev. C **96**, no. 2, 024004 (2017).
[7] E. Epelbaum, H.-W. Hammer, and U.-G. Meißner, Rev. Mod. Phys. 81, 1773 (2009).
[8] E. Epelbaum and U.-G. Meißner, Ann. Rev. Nucl. Part. Sci. **62**, 159 (2012).
[9] R. Machleidt and D. R. Entem, Phys. Rept. **503**, 1 (2011).
[10] D. Lonardoni, J. Carlson, S. Gandolfi, J. E. Lynn, K. E. Schmidt, A. Schwenk, and X. B. Wang, Phys. Rev. Lett. 120, (2018).
[11] M. Piarulli, A. Baroni, L. Girlanda, A. Kievsky, A. Lovato, E. Lusk, L. E. Marcucci, S. C. Pieper, R. Schiavilla, M. Viviani, and R. B. Wiringa, Phys. Rev. Lett. 120, 052503 (2018).
[12] G. Hupin, S. Quaglioni, and P. Navrátil, Phys. Rev. Lett. 114, (2015).
[13] P. Navrátil, V. G. Gueorguiev, J. P. Vary, W. E. Ormand, and A. Nogga, Phys. Rev. Lett. 99, (2007).
[14] E. Epelbaum *et al.*, arXiv:1807.02848 [nucl-th].
[15] A. Cipollone, C. Barbieri and P. Navrátil, Phys. Rev. C **92**, no. 1, 014306 (2015) doi:10.1103/PhysRevC.92.014306.
[16] G. Hagen, T. Papenbrock, D. J. Dean, and M. Hjorth-Jensen, Phys. Rev. Lett. 101, 092502 (2008).
[17] S. Binder, J. Langhammer, A. Calci, and R. Roth, Phys. Lett. B 736, 119 (2014).
[18] U.-G. Meißner, J. A. Oller, and A. Wirzba, Annals of Physics 297, 27 (2002).
[19] A. Lacour, J. A. Oller, and U.-G. Meißner, Annals of Physics 326, 241 (2011).
[20] K. Hebeler, S. K. Bogner, R. J. Furnstahl, A. Nogga, and A. Schwenk, Phys. Rev. C 83, 031301 (2011).
[21] A. Ekström, G. R. Jansen, K. A. Wendt, G. Hagen, T. Papenbrock, B. D. Carlsson, C. Forssén, M. Hjorth-Jensen, P. Navrátil, and W. Nazarewicz, Phys. Rev. C 91, (2015).
[22] D. Logoteta, I. Bombaci, and A. Kievsky, Phys. Lett. B 758, 449 (2016).
[23] C. Drischler, K. Hebeler, and A. Schwenk, ArXiv:1710.08220 (2017).
[24] G. Hagen, A. Ekström, C. Forssén, G. R. Jansen, W. Nazarewicz, T. Papenbrock, K. A. Wendt, S. Bacca, N. Barnea, B. Carlsson, C. Drischler, K. Hebeler, M. Hjorth-Jensen, M. Miorelli, G. Orlandini, A. Schwenk, and J. Simonis, Nature Physics 12, 186 (2016).
[25] G. Hagen, G. R. Jansen, and T. Papenbrock, Phys. Rev. Lett. 117, 172501 (2016).
[26] J. Simonis, S. R. Stroberg, K. Hebeler, J. D. Holt, and A. Schwenk, Phys. Rev. C 96, (2017).
[27] T. D. Morris, J. Simonis, S. R. Stroberg, C. Stumpf, G. Hagen, J. D. Holt, G. R. Jansen, T. Papenbrock, R. Roth, and A. Schwenk, Phys. Rev. Lett. 120, (2018).
[28] S. Elhatisari, N. Li, A. Rokash, J. M. Alarcón, D. Du, N. Klein, B. Lu, U.-G. Meißner, E. Epelbaum, H. Krebs, T. A. Lähde, D. Lee, and G. Rupak, Phys. Rev. Lett. 117, 132501 (2016).
[29] E. Wigner, Phys. Rev. **51**, 106 (1937).
[30] A. Rokash, E. Epelbaum, H. Krebs and D. Lee, Phys. Rev. Lett. **118**, 232502 (2017).
[31] L. Platter, H.-W. Hammer, and U.-G. Meißner, Phys. Lett. B 607, 254 (2005).
[32] N. Klein, S. Elhatisari, T. A. Lähde, D. Lee, and U.-G. Meißner, ArXiv:1803.04231 (2018).
[33] S. König, H. W. Grießhammer, H.-W. Hammer, and U. van Kolck, Phys. Rev. Lett. 118, 202501 (2017).
[34] A. Kievsky and M. Gattobigio, Few-Body Syst. 57, 217 (2016).
[35] S. Elhatisari, E. Epelbaum, H. Krebs, T. A. Lähde, D. Lee, N. Li, B. Lu, U.-G. Meißner, and G. Rupak, Phys. Rev. Lett. 119, 222505 (2017).
[36] B. Borasoy, E. Epelbaum, H. Krebs, D. Lee, and U.-G. Meißner, Eur. Phys. J. A 31, 105 (2007).
[37] N. Klein, D. Lee, and U.-G. Meißner, ArXiv:1807.04234 (2018).
[38] B.-N. Lu, T. A. Lähde, D. Lee, and U.-G. Meißner, Phys. Lett. B 760, 309 (2016).
[39] B. Borasoy, E. Epelbaum, H. Krebs, D. Lee, and U.-G. Meißner, Eur. Phys. J. A 31, 105 (2007).
[40] B. Borasoy, E. Epelbaum, H. Krebs, D. Lee, and U.-G. Meißner, Eur. Phys. J. A 35, 343 (2008).
[41] E. Epelbaum, H. Krebs, D. Lee, and U.-G. Meißner, Eur. Phys. J. A 41, 125 (2009).
[42] D. Lee, Prog. Part. Nucl. Phys. 63, 117 (2009).
[43] P. Möller, J. R. Nix, W. D. Myers, and W. J. Swiatecki, Atomic Data and Nuclear Data Tables 59, 185 (1995).
[44] N. Wang, M. Liu, X. Wu, and J. Meng, Phys. Lett. B 734, 215 (2014).
[45] M. Bender, P.-H. Heenen, and P.-G. Reinhard, Rev. of Mod. Phys. 75, 121 (2003).
[46] G. R. Jansen, J. Engel, G. Hagen, P. Navratil, and A. Signoracci, Phys. Rev. Lett. 113, 142502 (2014).
[47] M. Wang, G. Audi, F. G. Kondev, W. J. Huang, S. Naimi, and X. Xu, Chin. Phys. C 41, 030003 (2017).
[48] I. Angeli and K. P. Marinova, Atomic Data and Nuclear Data Tables 99, 69 (2013).
[49] H. De Vries, C. W. De Jager, and C. De Vries, Atomic Data and Nuclear Data Tables 36, 495 (1987).
[50] I. Tews, T. Krüger, K. Hebeler, and A. Schwenk, Phys. Rev. Lett. 110, (2013).
[51] A. Akmal, V. R. Pandharipande, and D. G. Ravenhall, Physical Review C 58, 1804 (1998).
[52] S. Gandolfi, J. Carlson, and S. Reddy, Phys. Rev. C 85, (2012).